DISTRIBUTIONAL CONCAVITY REGULARIZATION FOR GANS

Anonymous authors
Paper under double-blind review

ABSTRACT

We propose Distributional Concavity (DC) regularization for Generative Adversarial Networks (GANs), a functional gradient-based method that promotes the entropy of the generator distribution and works against mode collapse. Our DC regularization is an easy-to-implement method that can be used in combination with the current state of the art methods like Spectral Normalization and Wasserstein GAN with gradient penalty to further improve the performance. We will not only show that our DC regularization can achieve highly competitive results on ILSVRC2012 and CIFAR datasets in terms of Inception score and Fréchet inception distance, but also provide a mathematical guarantee that our method can always increase the entropy of the generator distribution. We will also show an intimate theoretical connection between our method and the theory of optimal transport.

1 INTRODUCTION

Generative Adversarial Networks (GANs) (Goodfellow et al., 2014) is a model consisting of two adversarial neural networks designed for the training of a generator distribution that mimics a target distribution defined on a (*often*) high dimensional space, and it has been successful in numerous applications including image and movie generations (Isola et al., 2017; Zhu et al., 2017; Saito et al., 2017). However, it has not yet completely established itself as a wieldly scientific tool because of the sheer computational difficulty of its training process. As such, there has been numerous studies seeking for a way to stabilize the training process of GANs (Gulrajani et al., 2017; Miyato et al., 2018; Karras et al., 2018).

Mode collapse is a persistent central problem for the training of GANs, which collectively refers to the lack of diversity in generator distribution. For instance, without any countermeasure, GANs applied to multimodal mixture of Gaussians will often train a generator distribution with one mode (See Fig 22, Goodfellow (2016) for example). Mode collapse has been discussed in numerous literatures related GANs. To name a few, see Goodfellow (2016); Metz et al. (2016); Arjovsky & Bottou (2017); Arjovsky et al. (2017); Lin et al. (2017).

In words of statistical machine learning, mode collapse can be described as a case of entropy degeneration. A naive countermeasure against mode collapse is therefore to augment the entropy of the generator distribution. Not many studies to date, however, tackled the problem of mode collapse using this direct approach. Dai et al. (2017) partially realized this idea by actually evaluating the entropy of the generator distribution with variational inference and including it into the objective function. This type of strategy requires the user to continuously produce reliable estimates of the generators based on finite samples throughout the course of the training. As such, not much further improvement can be expected from this strategy, because precise estimation of the entropy tends to be computationally heavy, and empirical estimation is an excruciatingly difficult problem on its own in high dimension, as is the case in image and movie generation. In fact, the performance of classical methods based on kernel density estimation, for example, does not scale well with respect to dimension, and the number of samples required to control the MSE can grow exponentially with the dimension (Cacoullos, 1966; Ozakin & Gray, 2009).

In this study, we use the theory of *functional gradient* to develop a method that can promote the entropy of the generator distribution without directly estimating the entropy itself. The functional

gradient of an objective function with respect to a model function is an *infinite dimensional gradient* computed over the infinite dimensional space of all models. As we will show, all variations of GANs to date are implicitly using the discriminator function to compute the *functional* derivative of the objective function with respect to the generator distribution function. In other words, the disrciminator determines the direction to which the algorithm should move the mass of the current generator distribution. The work of Nitanda & Suzuki (2018) is a pioneer study that explicitly incorporated this idea into the training of neural generator models. Their study showed that one can carry out a faithful functional gradient-based update by inserting what they call *gradient layer* into the layers of neural generator function. Johnson & Zhang (2018) further polished this strategy by periodically distilling the networks.

One advantage of the functional gradient-based approach is that, at every stage in the training process of the generator distribution, the user can monitor what the next (target) distribution looks like in terms of the current distribution. In contrast, the target distribution set forth by conventional parametric methods is usually expressed in a complicated parametric form (e.g. Deep Neural Nets (DNNs)), and its behaviors are often difficult to predict. This advantage of the functional gradient based-update suggests the possibility that we can control the update rule in order to deliberately direct the generator distribution to a distribution with preferred properties–which, in our case, include *high entropy*.

We discovered that, by locally concavifying the discriminator function, we can manipulate the funcational gradient so that the next update for the generator will always target a distribution with higher entropy. From now on, we should refer to our method by *Distributional Concavity (DC) regularization*. Our method does not require the direct estimation of the entropy. We will not only show that our DC regularization can help improve the performance of GANs in terms of Inception score (Salimans et al., 2016) and Fréchet inception distance (FID) (Heusel et al., 2017), but also give a mathematical guarantee that our regularization will always increase the entropy of the generator distribution. We will also show that our method greatly outperforms the method of Dai et al. (2017) that directly estimates the entropy based on classicaly techniques.

The regularization strategy of monotnically increasing the entropy of the generator distribution over the course of its training is *not* without theoretical basis. Our DC regularization has close relations to the theory of optimal transport. We will show that, when the entropy of the true distribution is higher than the current generator distribution, the functional gradient that is properly derived from the optimal mass transport always increases the entropy of the distribution. Moreover, the functional update used in our method is always a monotonic mapping, which also turns out to be one of the properties satisfied by the update with optimal transport. This is a preferred property as well, because it tends to promote the smooth training of the generator. We summarize our contributions below:

- We propose an update for the generator of GANs that promotes the entropy of the generator without the need for an explicit estimation of the actual entropy.
- We show that, when the entropy of the true distribution is larger than that of the current generator distribution, the functional gradient derived from the 2-Wasserstein (W_2) optimal transport always increases the entropy of the distribution.
- We provide a mathematical guarantee that our method increases the entropy of the generator distribution at every step.
- We show that our method improves the results of GANs in terms of Inception score and FID score.

2 THEORY

2.1 GENERATIVE ADVERSARIAL NETWORKS

Let us first review the formulation of the original GANs. Unless otherwise noted, let us use boldface capital letters to refer to a random variable, and lower case letter for its realization. The training process of GANs (Goodfellow et al., 2014) is a two player min-max game in which the generator distribution μ_θ is trained to minimize the *divergence* between the true distribution ν and the generator distribution μ_θ measured by the current critic F, while the critic F is trained to most strongly discriminate μ_θ from ν. Often, μ_θ is produced by applying a generator function G to a random seed variable with some distribution μ_z. In a nutshell, GANs aims to find optimal G^* that achieves the

minimum value for

$$\min_G \max_F \mathbb{E}_\nu[\mathcal{L}_r(F(\boldsymbol{X}))] + \mathbb{E}_{\mu_z}[\mathcal{L}_g(F(G(\boldsymbol{Z})))] := \min_G \max_F V(G,F) \tag{1}$$

where $\mathcal{L}_r$ and $\mathcal{L}_g$ are the functions of user's choice. We can retrieve the formulation of the original GAN by letting $\mathcal{L}_r(F(\boldsymbol{x})) = \text{softplus}(-F(\boldsymbol{x}))$ and $\mathcal{L}_g(F(\boldsymbol{x})) = \text{softplus}(F(\boldsymbol{x}))$, where $\text{softplus}(\cdot) = \log(1+\exp(\cdot))$. If we define the discriminator $\mathcal{D}(\boldsymbol{x})$ as $(1+\exp(-F(\boldsymbol{x})))^{-1}$, the training of $\mathcal{D}$ with the equation (1) emerges as the training of a classifier that distinguishes the samples of ν from the samples of μ_θ. It is known that the optimal $\mathcal{D}$ is given by $\mathcal{D}^*(\boldsymbol{x}) = \frac{\nu(\boldsymbol{x})}{\nu(\boldsymbol{x})+\mu_\theta(\boldsymbol{x})}$, and the problem of finding the optimal G^* in this case becomes the problem of finding the minimizer of Jensen Shannon divergence (Goodfellow et al., 2014). There is a variety of choices for $(\mathcal{L}_r, \mathcal{L}_g)$ (Arjovsky et al., 2017; Lim & Ye, 2017; Mao et al., 2017; Nowozin et al., 2016).

2.2 Functional Gradient interpretation of the GANs update

Next, we would provide an interpretation for the update rule of GANs from the perspective of functional gradient. For ease of argument, we will assume the followings from here onward. First, as is the case in many application of GANs, we will assume that ν is a probability measure on the Euclidean space $\mathbb{R}^d$, and μ_z is a probability measure on some Euclidean space U. Let us also assume that $G : U \to \mathbb{R}^d$ is a parametric function of θ that is almost everywhere differentiable with respect to both input and θ. We will first consider the optimization problem of the equation (1) with gradient descent about θ. For ease of notation, let us write $L = \mathcal{L}_g \circ F$. We will assume that L is a continuously differrentiable and uniformly bounded function on $\mathbb{R}^d$, and that the Euclidean norms of its gradient and operator norm of Hessian are also uniformly bounded. This type of regularity assumptions on the objective functions are used in other literatures as well (Nitanda & Suzuki (2018), Johnson & Zhang (2018)), and it is not too all unrealistic because the support of both target distributions and generator distribution are often compact throughout the course of the training in the real applications. We will also assume that the derivatives of all functions to appear are well defined and bounded on $\mathbb{R}^d$. The update rule of θ is given by:

$$\theta_{new} = \theta_{old} - \alpha \nabla_\theta \mathbb{E}_{\mu_z}[L(G(\boldsymbol{Z};\theta))]\big|_{\theta=\theta_{old}} \tag{2}$$

$$= \theta_{old} - \alpha\, \mathbb{E}_{\mu_z}\left[D_{\theta_{old}} G(\boldsymbol{Z};\theta_{old}) \nabla L(G(\boldsymbol{Z};\theta_{old}))\right] \tag{3}$$

where D_θ represents the derivative operator with respect to θ. In general, almost all variations of GANs to date (Arjovsky et al., 2017; Lim & Ye, 2017; Mao et al., 2017; Nowozin et al., 2016) uses this type of update rule for the training of the generator. Let us denote the law of $G(\boldsymbol{Z};\theta)$ (or $\boldsymbol{X}$) by μ_θ. Let $\mathcal{L}^2(\mu_\theta)$ denote the Hilbert space of L^2 integrable maps from $\mathbb{R}^d$ to itself, granted with the inner product $\langle a, b\rangle_{\mu_\theta} = E_{\mu_\theta}[a(\boldsymbol{X})^T b(\boldsymbol{X})]$. We will show that we can re-derive the equation (3) using the theory of functional gradient. To begin with, instead of updating the parameter θ, we would like to consider directly updating the distribution μ_θ by applying a $T \in \mathcal{L}^2(\mu_\theta)$ to a random variable generated from μ_θ. This will result in a new distribution $T\#\mu_\theta$, which is a unique distribution that satisfies $\mathbb{E}_{\mu_\theta}[h(T(\boldsymbol{X})] = \mathbb{E}_{T\#\mu_\theta}[h(\boldsymbol{X})]$ for all measurable h.

Now, in order to create an update rule for T, let us consider the Gâteaux derivative of $M(T) := E_{T\#\mu_\theta}[L(\boldsymbol{X})]$ with respect to T into an arbitrary direction $\delta \in \mathcal{L}^2(\mu_\theta)$. In terse term, we would like to consider the effect of purturbing T into the direction of δ. By the compactnesss assumption on Ω together with the regularity assumptions for the functions defined hereof, we can appeal to the dominated convergence theorem and see that

$$\lim_{\epsilon\to 0} \frac{M(T+\epsilon\delta) - M(T)}{\epsilon} = \mathbb{E}_{\mu_\theta}[\nabla L(T(\boldsymbol{X}))^T \delta(\boldsymbol{X})]. \tag{4}$$

is uniform for all $\delta \in \mathcal{L}^2(\mu)$. This way, the term $\nabla L(T(\cdot))$ in the expression above is a Fréchet derivative, or the type of derivative to which the usual set of derivative rules can be applied. We will refer to this derivative as *functional derivative* for short. Note that the *directional functional derivative* $\mathbb{E}_{\mu_\theta}[(\nabla L(T(\boldsymbol{X}))\cdot\delta)(\cdot)]$ will always take a positive value when $\delta \propto \nabla L(T(\cdot))$. Thus, for α small enough, an update from the current choice of T to $T - \alpha\nabla L \in \mathcal{L}^2(\mu_\theta)$ will decrease the objective function. Here, we are interested in the *derivative* computed at $T = Id$, so the transformation we would like to apply to μ_θ is

$$T_\alpha(\boldsymbol{x}) = \boldsymbol{x} - \frac{\alpha}{2}\nabla L(\boldsymbol{x}). \tag{5}$$

This is indeed a transportation of a mass into the direction of $\alpha \nabla L$. Now, for the update of θ, we would like to design θ_{new} such that $\mu_{\theta_{new}}$ is closer to the **target distribution** $T\#\mu_{\theta_{old}}$ than $\mu_{\theta_{old}}$. That is, we would like to choose θ that minimizes

$$\mathbb{E}_{\mu_z}[\|T_\alpha(G(\boldsymbol{Z};\theta_{old})) - G(\boldsymbol{Z};\theta)\|_2^2]. \tag{6}$$

The gradient of this sub-objective function with respect to θ is given by

$$2\mathbb{E}_{\mu_z}[D_\theta G(\boldsymbol{Z};\theta)(T_\alpha(G(\boldsymbol{Z};\theta_{old})) - G(\boldsymbol{Z};\theta_{old}))] = -\alpha \mathbb{E}_{\mu_z}[D_\theta G(\boldsymbol{Z};\theta)\nabla L(G(\boldsymbol{Z};\theta_{old})]. \tag{7}$$

Evaluating this at $\theta = \theta_{old}$, we recover the gradient used in the equation (3). This formulation is practically equivalent to the one introduced in xICFG (Johnson & Zhang, 2018).

2.3 Choice of the target distribution

From the perspective of functional gradient, the min-max game of GANs can be decomposed into (i) **the target construction step** that looks for a next *target distribution* in the vicinity of the current generator distribution that is closer to the true distribution than the current distribution, and (ii) **the distillation step** that looks for a neural function that better approximates the target distribution. Our proposal is to design a target distribution $T\#\mu_\theta$ with favorable properties. In this study, we would particularly like to design T that promotes higher entropy and satisfies monotonicity condition, which we will describe momentarily. Indeed, the promotion of entropy shall discourages mode collapse. Meanwhile, the monotonicity is a property that assures that there is no *crossings* in the transport:

$$\langle T(\boldsymbol{x}) - T(\boldsymbol{x}'), \boldsymbol{x} - \boldsymbol{x}' \rangle_{\mathbb{R}^d} \geq 0.$$

This is a preferred property because, as we will empirically show (see section 4.1) , the *crossings* in the transport tend to hinder the smooth training process. This is in fact somewhat intuitive, because crossings lead to wasteful transportation of the mass. As it turns out, we can satisfy both of these conditions by simply requiring L to be concave.

Proposition 2.1.
Let μ be a probability distribution on $\mathbb{R}^d$.
*If L is **concave** on the support of μ, then $H(T\#\mu) \geq H(\mu)$.*

Note that this statement is independent of the step size, because any positive scalar multiple of concave function is concave. Also, by definition, the concavity of L implies the strong convexity of T, and the strong convexity of T implies

$$\langle T(\boldsymbol{x}) - T(\boldsymbol{x}'), \boldsymbol{x} - \boldsymbol{x}' \rangle_{\mathbb{R}^d} \geq \|\boldsymbol{x} - \boldsymbol{x}'\|_2^2 \geq 0, \tag{8}$$

which is a stronger condition than the monotonicity. Thus, by simply making L concave, we can not only construct a target distribution whose entropy is greater than that of the current generatator distribution, but also assure that the corresponding transport is monotonic. The proposal we would like to make in this study is simply to choose a distribution constructed from concave L in the target construction step.

2.4 Relation to optimal transport

Our DC regularization has close relations to the theory of optimal transport. In fact, an equation of form 5 is ubiquitous in the theory of optimal transport. In order to further articulate this point, we would like to briefly introduce the notion of optimal transport. For more rigorous introduction of the concept, please consult (Villani, 2008).
For $p \geq 1$, the p-Wasserstein distance $W_p(\mu, \nu)$ between two arbitrary distributions μ and ν with sufficient regularity is given by

$$\left(\inf_T E_\mu[\|\boldsymbol{X} - T(\boldsymbol{X})\|_2^p]\right)^{1/\mathrm{p}}, \tag{9}$$

where the inf above is taken over all measurable maps T satisfying $T\#\mu = \nu$. When $p = 2$, it is known that the infimum of this cost function is achieved by T^* that can be expressed as $\boldsymbol{x} - \nabla L^*$ for some L^* that renders $\|\boldsymbol{x}\|^2/2 - L^*$ convex (Brenier, 1991). The search for L^* and hence T^* therefore amounts to the search for the closest coupling between μ and ν in the L_2 sense. One surprising fact is that the movement of the particle along the direction of ∇L^* monotonically decreases W_2

(Villani, 2008). That is, if $T_t^*(\boldsymbol{x}) = \boldsymbol{x} - t\nabla L^*(\boldsymbol{x})$, then $W_2(T_t^*\#\mu, \nu)$ monotonically decreases with t (Villani, 2003). Please compare this transport equation with the equation (5). This T_t^* is indeed the optimal transportation analogue of the functional gradient. The theorem in Brenier (1991) has a still surprising converse; for any convex function L, $T = \boldsymbol{x} - \nabla L$ turns out to be *the* unique optimal transport from μ to $T\#\mu$. Using this fact, we can appeal to the following proposition 2.4 to claim that the functional update based on the optimal transport satisfies one important property that shall be intuitively fulfilled if we are in fact moving the distribution toward the true distribution—that is, if the current distribution has lower entropy than the true distribution, the sequence of the distributions produced by the updates should be monotonically increasing in the entropy:

Proposition 2.2.
Suppose $\nu = T\#\mu$ for some T that can be written as a gradient of a strictly convex function. If $H(\nu) \geq H(\mu)$, then $H(T_t\#\mu)$ is monotonically increasing on $t \in [0, 1]$.

This proposition actually assures that the updates of DC regularization also satisfy the same property. Because we are designing the target distribution so that it will have higher entropy than the current distribution at every step, by letting ν in the proposition 2.4 to be the target distribution, we have a guarantee that the sequence of distributions constructed by our updates is also monotnically increasing in the entropy. To see this, simply note that we can automatically make $\|\boldsymbol{x}\|^2/2 - L$ to be convex by making L concave,

The connection between our DC regularization and optimal transport is not limited to the property we introduced above. By the theory of Brenir, the choice $T_\alpha = Id - \alpha^{1/2}\nabla L$ with concave and 1-Lipshitz L satisfies $W_2(\mu, T_\alpha\#\mu) = \sqrt{E[\|\alpha^{1/2}\nabla L(\boldsymbol{X})\|_2^2]} = \alpha$. Put in still other words, by constructing a target distribution with concave L, we can also assure that the target distribution is contained within the W_2 neighborhood of the current distribution function. This is a property that cannot be guaranteed with the conventional parameter-based updates. Monotonicity condition is also a property that is satisfied by the optimal transport. According the theory of Monge-Ampere (Villani (2008)), a transport map can be optimal only if it is monotonic. Thus, while not being exactly based on the optimal transport from the generator distribution to the true distribution, our T shares many favorable properties in common with the optimal transport, and is very closely related to the theory of W_2 distance.

Reflecting on these facts, one might become tempted to say that we shall simply formulate GANs with the objective function that is solely based on W_2 distance between the generator distribution and the true distribution. However, as we will further articulate in the discussion section, the challenge remains to conduct faithful W_2-based updates in the implementation of GANs.

3 METHOD

If $\mu_\theta := G_\theta\#\mu_z$ is our current parametric generator distribution and ν is the true distribution, our DC regularization method first (i) proposes a target distribution $T\#\mu_\theta$ using a concave L, and then (ii) seek a measure $\mu_{\theta_{new}}$ that well approximates the target distribution $T\#\mu_\theta$. We use the following sampling-based penalty term in order to promote the concavity of L:

$$\mathcal{L}_{dc}(F, \epsilon, \boldsymbol{x}_1, \boldsymbol{x}_2, d) = \max\{L(\epsilon\boldsymbol{x}_1 + (1-\epsilon)\boldsymbol{x}_2) - \epsilon L(\boldsymbol{x}_1) - (1-\epsilon)L(\boldsymbol{x}_2), d\}, \qquad (10)$$

where $\boldsymbol{x}_1, \boldsymbol{x}_2$ are samples from the support of μ_θ, ϵ is a sample from the uniform distribution over $[0, 1]$, and d is a positive scalar. Note that this term must be positive if L is concave over the support of μ_θ. Our algorithm is summarized in Algorithm 1. The update rule in this algorithm uses the target distribution constructed by $T(\boldsymbol{x}) = \boldsymbol{x} - \nabla L$ with concave L. Intuitively speaking, the transport T has an effect of moving μ_θ toward $T\#\mu_\theta$ while dispersing the mass of μ_θ. See Fig 1 for a visual rendering of this interpretation.

In most practical application, the training of GANs begins by dispersing the initial distribution with small entropy and gradually molds the mass into what resembles the true distribution. Our transport ensures that this *dispersion* is consistently happening over the course of the training. As we will show in the result section, this regularization works in favor of the inception score without any noticeable downfall from *over-dispersion*, suggesting that the generator distribution created with the current state of the art techniques are still not *dispersed enough*.

Algorithm 1 GANs algorithm with DC regularization

for each iteration **do**

$\theta_{old} \leftarrow \theta$

the target construction step : update critic by critic's objective

$$\max_{F} V(G,F) + \lambda \mathbb{E}_{\text{Uniform}(\epsilon)} \mathbb{E}_{\mu_{\theta_{old}}(\boldsymbol{X}_1,\boldsymbol{X}_2)}[\mathcal{L}_{dc}(F,\boldsymbol{\epsilon},\boldsymbol{X}_1,\boldsymbol{X}_2,d)] \tag{11}$$

the distillation step : update generator by generator's objective

$$\min_{\theta} \mathbb{E}_{\mu_z}[\|T(G(\boldsymbol{Z};\theta_{old})) - G(\boldsymbol{Z};\theta)\|^2] \tag{12}$$

end for

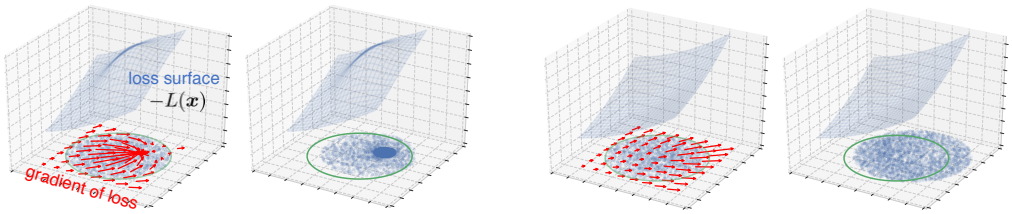

(a) $-L$ is not convex (b) $-L$ is convex

Fig 1: The graph of $-L$ and its gradient vector field. Each point $\boldsymbol{x}$ will be transported by T along the direction of the vector field $-\nabla L$. Over the set on which L is not concave, T may move the points in the region come closer to each other. The use of concavified L for the construction of transport function will make the points move away from each other.

4 Experimental Results

We applied DC regularization to the training of GANs on CIFAR-10 (Torralba et al., 2008), CIFAR-100 (Torralba et al., 2008) and ILSVRC2012 dataset (ImageNet) (Russakovsky et al., 2015) in various settings and evaluated its performance in terms of Inception score (Salimans et al., 2016) and *Fréchet inception distance* (FID) (Heusel et al., 2017). Inception score and FID are performance measures that are commonly used to evaluate the severity of mode collapse. For the details of the evaluation, see Appendix B.1. We also conducted an additional set of experiments with artifical dataset to investigate the properties of DC-regularization. We provide the results for additional experiments in the Appendix C as well.

4.1 Intrinsic properties of DC regularization

Effect of DC regularization on entropy

Using a simple Gaussian Mixture Model as the true distribution, we evaluated the sheer ability of the DC regularization to promote the entropy of the generator distribution. We used hinge loss for the objective function, and used DNNs to model both the discriminator and the generator. We trained the model with and without the DC regularization and reported the entropy of the Generator at different stages of the training by explicitly computing the determinant of the Jacobian at each layer. The result is illustrated in Fig 2 (a). We see that the regularization is positively affecting the entropy at all stages of the training. Indeed, the persistent pressure to increase the entropy can result in over-dispsersed final product. However, this seems not to be a serious issue when it comes to the learning on big data like ImageNet. In terms of Inception score and FID score, all artificial generator distributions today are still far less diverse than the original dataset (Table 1), and there is still a large room left for the improvement of diversity.

Effect on monotonicity

We also made an assessment on the effect of choosing a target distribution constructed with monotonic mapping. Let K be a positive value. Starting from the initial distribution $X = G_{\theta_0}(Z)$, consider the following pair of maps to be applied to X:

$$T^{(m)}(x) = (x-K)\mathbb{1}_{(-1)^m x \leq 0} + (x+K)\mathbb{1}_{(-1)^m x \geq 0} \tag{13}$$

It is evident that $T^{(2)}$ is a monotonic mapping and $T^{(1)}$ is not. Denote the law of X by μ. We used $T^{(1)}\#\mu$ and $T^{(2)}\#\mu$ as target distributions, and trained the θ using $O_m = E_Z[\|T^{(m)}(G_{\theta_0}(Z)) - G_\theta(Z)\|^2]$ as the objective function. Note that, for both $m = 1, 2$, this objective function takes the same value, K^2. However, as we can see in Fig 2 (b), the training with O_2 proceeds much faster than the training with O_1. This outcome is against a naive intuition based on distributional distance because the $W_2(T^{(1)}\#\mu, \mu) < W_2(T^{(2)}\#\mu, \mu)$. To see this, note that T_1 is a derivative of $-K|X|$ and $T^{(2)}$ is a derivative of $K|X|$, which is a convex function. This implies that $T^{(2)}$ is *the* optimal transport from μ to $T^{(2)}\#\mu$. On the other hand, by the definition of the Wasserstein distance, $K = W_2(T^{(2)}\#\mu, \mu)$ while $W_2(T^{(1)}\#\mu, \mu)^2 = \inf_{T\#\mu = T_1\#\mu} E_\mu[\|T(X) - X\|^2] \leq E_\mu[\|T^{(1)}(X) - X\|^2] = K^2$. This result (Fig 2 (b)) suggests that, when using the update rule similar to the equation 3, the training proceeds much faster when we choose a target distribution with monotonic mapping.

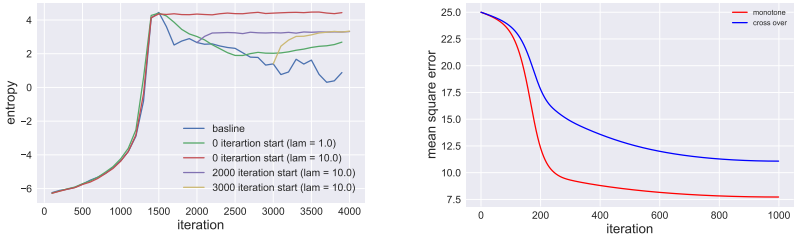

(a) Effect on entropy (b) Effect on monotonicity

Fig 2: The effect of DC regularization on entropy and monotonicity.

4.2 Results on CIFAR-10 and CIFAR-100

Experiments with different architectures and objective functions

We tested our algorithm for the training of GANs with six types of objective functions and two network architectures, and reported the performance on all 12 combinations. For the details of the objective functions and the architectures, please see Appendix B.2, B.3, B.4 For the training of the network, we applied Spectral Normalization (SN) (Miyato et al., 2018) to the full-connected layer and the convolution layer. Fig 3 and Fig 8 (in Appendix) respectively summarize Inception scores and FID for all 12 settings. We see that DC regularization is improving the performance irrespective of the choice of the architecture and the objective function.

Experiments with different prior dimensions

In general, without careful selection of the dimension of the prior distribution, the training of GANs tends to suffer a serious case of mode collapse. For image generation task, this will result in low inception score. We therefore applied DC regularization to the trainings of GANs on CIFAR-10 with very low prior dimensions as well as very large prior dimensions and evaluated the performance. For this experiment, we used GAN-variant2 (Appendix B.2) for the objective function and used SND-CGAN for the architecture. As for the experimental details, please see Appendix B.4. The results are summarized in Fig 4 and Fig 10 (in Appendix). When the prior dimension is below the inherent dimension of the dataset, the dimension of the generator distribution cannot match the dimension of the true distribution. Thus, the inception score of the generator trained with low dimensional prior is bound to be low, irrespective of the application of DC regularization. However, for $\dim(\boldsymbol{z}) \geq 5$, the inception score is as high as 7.5, and for all choices of $\dim(\boldsymbol{z})$, the generator trained with DC regularization consistently outperformed the generator trained without the DC regularization. Similar argument applies to the performance of DC regularization for high dimensional prior. Overall, the DC regularization provides some robustness against the choice of the prior dimension.

Comparison with EGAN and other methods

We compared the performance of our algorithm against EGAN (Dai et al., 2017), another framework that can be used to control the entropy of the generator. In particular, we implemented EGAN-Ent-VI, which includes into its objective function a penalty against the negative entropy of the generator. We conducted this comparative study using SNDCGAN (Table 2) and SNResNet (Table 3). For the experimental setting of this study, please see the Appendix B.4. As we show in Table 1, DC

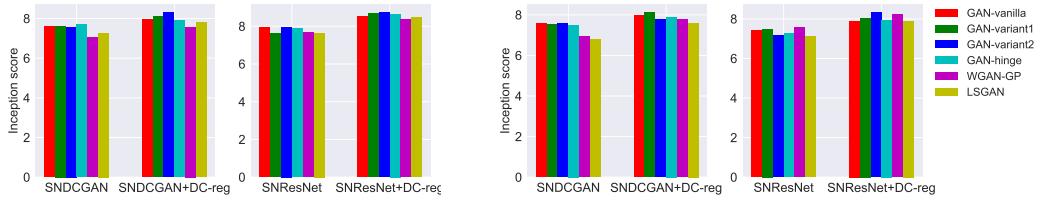

(a) CIFAR-10 (b) CIFAR-100

Fig 3: Inception scores on CIFAR-10 and CIFAR-100 (higher the better).

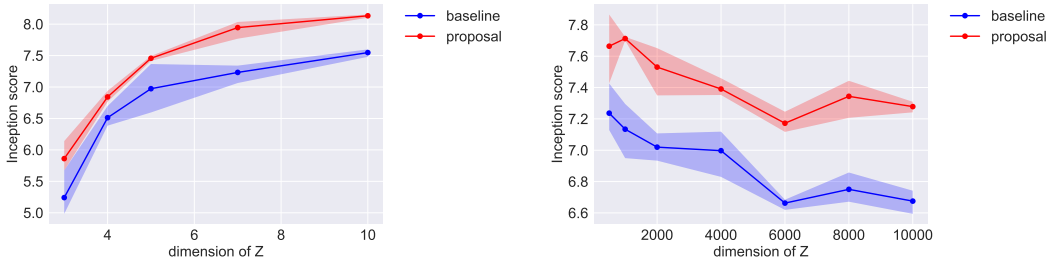

(a) low prior dimension (b) high prior dimension

Fig 4: Effect of the prior dimension on the performance of DC regularization.

regularization outperformed EGAN-Ent-VI on both models. For the full version of the Table and the visuals of the generated samples, please see Table 8 and Table 11 in the Appendix. We would like to emphasize here that EGAN-Ent-VI requires a separate decoder in addition to the generator and the discriminator, and that our algorithm is easier to implement. We compared our algorithm against other competitive methods as well. The best performance of our method is almost on par with the state-of-the-art method (Karras et al., 2018). We are losing to progressive GAN (Karras et al., 2018) by a slight margin; we, however, would like to make a disclaimer that we are using much smaller architecture than Karras et al. (2018) for the performance evaluation of our method. We also comfirmed that we can improve the result of Miyato et al. (2018) by using DC regularization together with SN. The results support that our method is helping the training process suppress *mode collapse* and is improving the overall performance. For the results of the experiments conducted with Wasserstein GAN with gradient penalty (WGAN-GP) (Gulrajani et al., 2017), please see the Fig 9 in Appendix.

Table 1: Inception scores and FIDs for unsupervised image generation on CIFAR-10 and CIFAR-100. The CIFAR-10 results for the models designated with † are cited from (Miyato et al., 2018), and the CIFAR-10 results with ‡ are cited from (Karras et al., 2018).

Method	**Inception score**		**FID**	
	CIFAR-10	CIFAR-100	CIFAR-10	CIFAR-100
Real data	11.24	14.79	7.6	8.94
EGAN-Ent-VI(SNDCGAN)	6.95±.08	6.62±.10	29.0	33.3
EGAN-Ent-VI(SNResNet)	7.31±.12	6.67±.10	27.0	30.5
proposal				
SNDCGAN + DC reg	8.08±.12	8.12±.11	24.6	25.8
SNResNet + DC reg	8.27±.08	8.27±.13	24.3	24.6
SNResnetLarge + DC reg	8.41±.10	8.20±.08	20.6	24.8
SNResnetLarge-hinge + DC reg	8.29±.09	**8.41**±.11	**19.5**	**23.6**
baseline				
SNDCGAN†	7.42±.08	7.74±.08	29.3	27.9
SNDCGAN-hinge†	7.58±.12	7.57±.07	25.5	28.1
SNResnetLarge-hinge†	8.22±.05	7.54±.13	21.7	26.6
Progressive GANs‡	**8.56**±.06			

4.3 RESULTS ON IMAGENET

Additionaly, to evaluate our method's effectiveness on a higher dimensional dataset, we applied our method on ImageNet with 1000 classes, with each class containing approximately 1300 images. We compressed the images to 64×64 pixels prior to the experiments. For the objective function, we chose *GAN-hinge* (Appendix B.2), which was being used in Miyato et al. (2018). For the experimental settings, please see Appendix B.5 for the details. We can confirm on Fig 5 that our DC regularization is improving the Inception score throughout the course of the training.

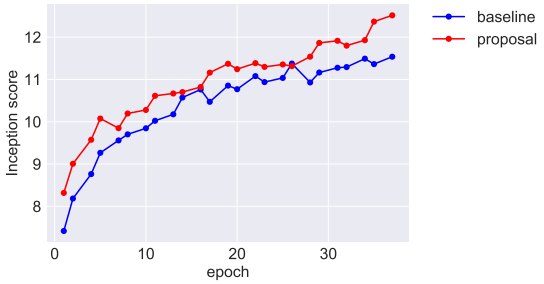

Fig 5: Performance of DC regularization on ImageNet.

5 DISCUSSION

Dilemma of GANs update
As we have shown above, the experimental results support our claim that the DC regularization promotes the entropy of the generator distribution and stabilizes the training process of GANs. As mentioned briefly in the theory section 2, however, we do not have the guarantee that our update rule consistently reduces the W_2 distance between the generator distribution and the true distribution. This fault, however, is common to almost all GANs algorithms today. As we have shown, the conventional update rule is implicitly targetting a distribution of the form $T\#\mu$ where $T = Id - \alpha\nabla L$ for some α and a discriminator L. As it turns out, optimal transport takes this form only when we are optimizing W_2 distance, while the common constraint of $|\nabla L| = 1$ is a condition required for dual potential when $p = 1$ (W_1) (Villani, 2008). In other words, the conventional GANs are making the discriminator with W_1 criteria and updating the generator with W_2 criteria. If we are to faithfully create the discriminator with W_2 criteria, we must look for a legendre-pair of dual potential functions. On the contrary, if we are to update the generator with W_1 criteria, one must look for a closed form solution for the W_1 transport. This, however, is in general a highly complex mathematical problem for which there is a separate field of study (Santambrogio, 2015). To the authors' best knowledge, no studies have provided a solid solution to this dilemma.

Convexity vs Strong convexity
We would like to also mention that our regularization is asking for more than what is required by W_2 theory. As mentioned above, in order for T to be the optimal transport from μ to $T\#\mu$, T only needs to be the gradient of a convex function. On the other hand, by asking L to be concave, we are in fact asking for T to be the gradient of a strongly convex function. This "overdo" is actually intentional. Recall that the parameter α in the transport $T_\alpha = Id - \alpha\nabla L$ corresponds to a step size in the update of the generator. If we train L that only guarantees the convexity of $\|\boldsymbol{x}\|^2/2 - L(\boldsymbol{x})$, the functional update derived from such L can be non-monotonic when the step size is large, because such L only guarantees the convexity of $\|\boldsymbol{x}\|^2/2 - \alpha L(\boldsymbol{x})$ when $\alpha \leq 1$. Should we require L to be concave, however, $\|\boldsymbol{x}\|^2/2 - \alpha L(\boldsymbol{x})$ is concave for any positive α. In this context, we may therefore say that the DC regularization leaves much room to be playful about the learning schedule. Finally, as can be inferred from our proofs for the proposition 2.3 and 2.4, the strong convexity of T has an effect of diffusing the mass of pdf in every direction. We can therefore expect the DC regularization to disperse the collapsed masses in the case of mode collapse. In the light of the fact that the training of GANs usually begins with dense distribution with small support, this dispersion effect should be helpful at the early stage of the training as well.

REFERENCES

Martin Arjovsky and Léon Bottou. Towards principled methods for training generative adversarial networks. In *ICLR*, 2017.

Martin Arjovsky, Soumith Chintala, and Léon Bottou. Wasserstein generative adversarial networks. In *ICML*, pp. 214–223, 2017.

Yann Brenier. Polar factorization and monotone rearrangement of vector-valued functions. *Communications on pure and applied mathematics*, 44(4):375–417, 1991.

Theophilos Cacoullos. Estimation of a multivariate density. *Annals of the Institute of Statistical Mathematics*, 18(1):179–189, 1966.

Zihang Dai, Amjad Almahairi, Philip Bachman, Eduard Hovy, and Aaron Courville. Calibrating energy-based generative adversarial networks. In *ICLR*, 2017.

DC Dowson and BV Landau. The fréchet distance between multivariate normal distributions. *Journal of Multivariate Analysis*, 12(3):450–455, 1982.

Ian Goodfellow. Nips 2016 tutorial: Generative adversarial networks. *arXiv preprint arXiv:1701.00160*, 2016.

Ian Goodfellow, Jean Pouget-Abadie, Mehdi Mirza, Bing Xu, David Warde-Farley, Sherjil Ozair, Aaron Courville, and Yoshua Bengio. Generative adversarial nets. In *NIPS*, pp. 2672–2680, 2014.

Ishaan Gulrajani, Faruk Ahmed, Martin Arjovsky, Vincent Dumoulin, and Aaron Courville. Improved training of wasserstein GANs. In *NIPS*, pp. 5769–5779, 2017.

Martin Heusel, Hubert Ramsauer, Thomas Unterthiner, Bernhard Nessler, Günter Klambauer, and Sepp Hochreiter. GANs trained by a two time-scale update rule converge to a nash equilibrium. In *NIPS*, pp. 6629–6640, 2017.

Phillip Isola, Jun-Yan Zhu, Tinghui Zhou, and Alexei A Efros. Image-to-image translation with conditional adversarial networks. In *CVPR*, pp. 5967–5976, 2017.

Rie Johnson and Tong Zhang. Composite functional gradient learning of generative adversarial models. In *ICML*, pp. 2376–2384, 2018.

Tero Karras, Timo Aila, Samuli Laine, and Jaakko Lehtinen. Progressive growing of gans for improved quality, stability, and variation. In *ICLR*, 2018.

Diederik Kingma and Jimmy Ba. Adam: A method for stochastic optimization. In *ICLR*, 2015.

Jae Hyun Lim and Jong Chul Ye. Geometric GAN. *arXiv preprint arXiv:1705.02894*, 2017.

Zinan Lin, Ashish Khetan, Giulia Fanti, and Sewoong Oh. Pacgan: The power of two samples in generative adversarial networks. *arXiv preprint arXiv:1712.04086*, 2017.

Xudong Mao, Qing Li, Haoran Xie, Raymond YK Lau, Zhen Wang, and Stephen Paul Smolley. Least squares generative adversarial networks. In *ICCV*, pp. 2813–2821, 2017.

Luke Metz, Ben Poole, David Pfau, and Jascha Sohl-Dickstein. Unrolled generative adversarial networks. *arXiv preprint arXiv:1611.02163*, 2016.

Takeru Miyato, Toshiki Kataoka, Masanori Koyama, and Yuichi Yoshida. Spectral normalization for generative adversarial networks. In *ICLR*, 2018.

Atsushi Nitanda and Taiji Suzuki. Gradient layer: Enhancing the convergence of adversarial training for generative models. In *AISTATS*, pp. 1008–1016, 2018.

Sebastian Nowozin, Botond Cseke, and Ryota Tomioka. f-GAN: Training generative neural samplers using variational divergence minimization. In *NIPS*, pp. 271–279, 2016.

Arkadas Ozakin and Alexander G Gray. Submanifold density estimation. In *Advances in Neural Information Processing Systems*, pp. 1375–1382, 2009.

Alec Radford, Luke Metz, and Soumith Chintala. Unsupervised representation learning with deep convolutional generative adversarial networks. In *ICLR*, 2016.

Olga Russakovsky, Jia Deng, Hao Su, Jonathan Krause, Sanjeev Satheesh, Sean Ma, Zhiheng Huang, Andrej Karpathy, Aditya Khosla, Michael Bernstein, Alexander C. Berg, and Li Fei-Fei. Imagenet large scale visual recognition challenge. *International Journal of Computer Vision*, 115(3):211–252, 2015.

Masaki Saito, Eiichi Matsumoto, and Shunta Saito. Temporal generative adversarial nets with singular value clipping. In *ICCV*, pp. 2849–2858, 2017.

Tim Salimans, Ian Goodfellow, Wojciech Zaremba, Vicki Cheung, Alec Radford, and Xi Chen. Improved techniques for training GANs. In *NIPS*, pp. 2226–2234, 2016.

Filippo Santambrogio. Optimal transport for applied mathematicians. *Birkäuser, NY*, pp. 99–102, 2015.

Christian Szegedy, Wei Liu, Yangqing Jia, Pierre Sermanet, Scott Reed, Dragomir Anguelov, Dumitru Erhan, Vincent Vanhoucke, and Andrew Rabinovich. Going deeper with convolutions. In *CVPR*, pp. 1–9, 2015.

Antonio Torralba, Rob Fergus, and William T Freeman. 80 million tiny images: A large data set for nonparametric object and scene recognition. *IEEE Transactions on Pattern Analysis and Machine Intelligence*, 30(11):1958–1970, 2008.

Cédric Villani. *Topics in Optimal Transportation*. Graduate studies in mathematics. American Mathematical Society, 2003.

Cédric Villani. *Optimal transport: old and new*, volume 338. Springer Science & Business Media, 2008.

Jun-Yan Zhu, Taesung Park, Phillip Isola, and Alexei A Efros. Unpaired image-to-image translation using cycle-consistent adversarial networks. In *ICCV*, pp. 2242–2251, 2017.

Appendix (Supplemental Material for Distributional Concavity Regularization for GANs)

A THE PROOFS FOR THE PROPOSITIONS 2.3 AND 2.4

We will first prove the proposition 2.4. Let us begin with a useful lemma. We will assume that all regularity assumptions made in Section 2 holds for all variables and functions that appear in this section. Also, we will use the Df to denote the derivative of f. Also assume that, unless otherwise noted, $Df(x)$ indicates $D_x f(x)$, the derivative of f with respect to x.

Lemma A.1. *Let μ and ν be probability distributions on $\mathbb{R}^n$, and suppose that we can write $(Id - \nabla L)\#\mu = \nu$ with one-to-one ∇L. Let us also write $T = (Id - \nabla L)$, and let $T_t = Id - t\nabla L$ be its time-linear interpolation. Then, for all $t \in [0, 1]$,*

$$\frac{d}{dt} H(T_t \# \mu) = -E_\mu \left[tr(I - tD^2 L(\boldsymbol{X}))^{-1} (D^2 L(\boldsymbol{X})) \right]. \tag{14}$$

Proof. Let p_μ be the pdf of μ. If $\boldsymbol{y} = T(\boldsymbol{x})$, by the one-to-one assumption $\det(DT(\boldsymbol{x})) > 0$ and we may let $d\boldsymbol{y} = \det(DT(\boldsymbol{x}))d\boldsymbol{x}$. By appealing to the fact that $E_\mu[h(T(\boldsymbol{X}))] = E_\nu[h(\boldsymbol{Y})]$ for arbitrary h,

$$\int h(T(\boldsymbol{x}))p_\mu(\boldsymbol{x})d\boldsymbol{x} = \int h(\boldsymbol{y})p_{T\#\mu}(\boldsymbol{y})dy = \int h(T(\boldsymbol{x}))p_{T\#\mu}(T(\boldsymbol{x}))\det(DT(\boldsymbol{x}))d\boldsymbol{x} \tag{15}$$

and we can deduce the identity $p_{T\#\mu}(T(\boldsymbol{x}))\det(DT(\boldsymbol{x})) = p_\mu(\boldsymbol{x})$. Building on this fact, with straightforward computation we can say

$$\begin{aligned} H(T_t\#\mu) &= -E_{T_t\#\mu}[\log p_{T_t\#\mu}(\boldsymbol{X})] && (16)\\ &= -\int p_\mu(\boldsymbol{x}) \log p_{T\#\mu}(T_t(\boldsymbol{x}))d\boldsymbol{x} && (17)\\ &= -\int p_\mu(\boldsymbol{x}) \left(\log p_\mu(\boldsymbol{x}) - \log\det(DT_t(\boldsymbol{x}))\right) d\boldsymbol{x} && (18)\\ &= H(\mu) + E_\mu \left[\log\det(DT_t(\boldsymbol{X}))\right]. && (19) \end{aligned}$$

Assuming that the distributions are regular enough that we can swap the integral, we can appeal to Jacobi's formula and deduce

$$\begin{aligned} \frac{d}{dt}H(T_t\#\mu) &= \frac{d}{dt}E_\mu \left[\log\det(DT_t(\boldsymbol{X}))\right] && (20)\\ &= \frac{d}{dt}E_\mu \left[\log\det(I - tD^2L(\boldsymbol{X}))\right] && (21)\\ &= E_\mu \left[\frac{\det(DT_t(\boldsymbol{X}))\mathrm{tr}(I - tD^2L(\boldsymbol{X}))^{-1}(-D^2L(\boldsymbol{X}))}{\det(DT_t(\boldsymbol{X}))}\right] && (22)\\ &= -E_\mu \left[\mathrm{tr}(I - tD^2L(\boldsymbol{X}))^{-1}(D^2L(\boldsymbol{X}))\right]. && (23) \end{aligned}$$

□

Now, let us prove the proposition 2.4. Without loss of generality, choose L so that $DT = \frac{\|\boldsymbol{x}\|^2}{2} - L$. Assuming that D^2L is diagonalizable and that its spectrum is uniformly bounded away from 1, let $\mathrm{spec}(D^2L) = \{\lambda_k\}$ and write $\mathrm{diag}\{\lambda_k\}_k = \Lambda$. Because $\frac{\|\boldsymbol{x}\|^2}{2} - L$ is assumed to be strictly convex, $D^2\left(\frac{\|\boldsymbol{x}\|^2}{2} - L\right) = I - D^2L$ is positive definite, and $1 - \lambda_k(\boldsymbol{x}) > 0$ for all k. Appealing to the line equation (19) we see that the assumption $H(\nu) > H(\mu)$ is equivalent to

$$\begin{aligned} E_\mu \left[\log\det(T(\boldsymbol{X}))\right] &= E_\mu \left[\log\det(I - D^2L(\boldsymbol{X}))\right]\\ &= E_\mu \left[\sum_k \log(1 - \lambda_k(\boldsymbol{X}))\right]. && (24)\\ &> 0 \end{aligned}$$

Let us write $max_k\{1 - t\lambda_k(\boldsymbol{x})\} = C_t(\boldsymbol{x}) > 0$. Using the assumption that the support of μ is compact, we can also say $0 < \max_{\text{supp}(\mu)}\{C_t(\boldsymbol{x})\} := c_t < \infty$. In general, if A is positive definite and diagonalizable, with straightforward argument we can say

$$\log(\det A) \leq \text{tr}(A - I) \tag{25}$$

Using this fact, we see that

$$\begin{aligned} 0 &< E_\mu \left[\log\det(I - D^2L(\boldsymbol{X}))\right] && (26)\\ &\leq E_\mu \left[\text{tr}(-D^2L(\boldsymbol{X}))\right] && (27)\\ &= E_\mu \left[\sum_k -\lambda_k(\boldsymbol{X})\right] && (28) \end{aligned}$$

Suppose that D^2L is diagonalizable with the change of basis matrix P. Then

$$\begin{aligned} -E_\mu \log\left[\text{tr}\left((I - tD^2L(\boldsymbol{X}))^{-1}D^2L(\boldsymbol{X})\right)\right] &= -E_\mu \left[\text{tr}\left((P^{-1}(I - t\Lambda)P)^{-1}P^{-1}\Lambda(\boldsymbol{X})P\right)\right] && (29)\\ &= -E_\mu \left[\text{tr}\left(P^{-1}(I - t\Lambda)^{-1}PP^{-1}\Lambda(\boldsymbol{X})P\right)\right] && (30)\\ &= -E_\mu \left[\text{tr}\left((I - t\Lambda(\boldsymbol{X}))^{-1}\Lambda(\boldsymbol{X})\right)\right] && (31)\\ &= -E_\mu \left[\sum_k \frac{\lambda_k(\boldsymbol{X})}{1 - t\lambda_k(\boldsymbol{X})}\right] && (32)\\ &\geq -E_\mu \left[\sum_k \frac{\lambda_k(\boldsymbol{X})}{c_t}\right] && (33)\\ &> 0 && (34) \end{aligned}$$

This concludes the proof of the proposition 2.4. The proposition 2.3 is much simpler to prove. In order to assure the $H(\nu) \geq H(\mu)$, we only need to guarantee that $E_\mu\left[\log\det(DT(\boldsymbol{X}))\right] \geq 0$. By requiring L to be concave, we would make $\|\boldsymbol{x}\|^2/2 - L(\boldsymbol{x})$ to be convex so that the eigenvalues of DT will all become positive. The result then follows trivially from the argument similar to the one that leads to equation (24).

B Experimental Settings

B.1 Performance measures

For the measure of GANs' performance on the image dataset, we used Inception score (Salimans et al., 2016). Inception score was introduced originally as an exponentiated divergence measure based on the trained Inception convolutional neural network (Szegedy et al., 2015), which is often called *Inception Model*. Using $p(y|\boldsymbol{x})$ to denote the Inception model, the inception score is given by $I(\{\boldsymbol{x}_n\}_{n=1}^N) := \exp(\hat{\mathbb{E}}[D_{\text{KL}}[p(y|\boldsymbol{x})||p(y)]])$, where $\hat{E}$ indicates the empirically approximated expectation. Often times, $p(y)$ is approximated with $\frac{1}{N}\sum_{n=1}^N p(y|\boldsymbol{x}_n)$.

The dominating consensus among the machine learning community is that this score is strongly correlated with subjective human judgment of image quality. Following the procedure in Salimans et al. (2016), we generated 5000 examples from each trained generator and calculated the Inception score on the samples. We evaluated the score 10 times with different seeds for the generation of x_n and reported the average and the standard deviation of the scores.

Fréchet inception distance (FID) (Heusel et al., 2017) is another measure for the quality of the generated examples that uses 2nd order information of the final layer of the inception model. The FID is based on *Freć́het distance* (Dowson & Landau, 1982) (Not to be confused with FID), which is the 2-Wasserstein distance between two distribution multivariate Gaussian distributions, p_1 and p_2. The Wasserstein distance for two Gaussian distributions have a closed form, and is given by

$$F(p_1, p_2) = \|\boldsymbol{\mu}_{p_1} - \boldsymbol{\mu}_{p_2}\|_2^2 + \text{trace}\left(C_{p_1} + C_{p_2} - 2(C_{p_1}C_{p_2})^{1/2}\right), \tag{35}$$

where $\{\boldsymbol{\mu}_{p_1}, C_{p_1}\}$, $\{\boldsymbol{\mu}_{p_2}, C_{p_2}\}$ are the mean and covariance of samples from q and p, respectively. Now, if $f_\ominus$ is the output of the final layer of the inception model before the softmax, the Fréchet

inception distance (FID) between two distributions p_1 and p_2 on the images is the *Freć het distance* distance between $f_\ominus \circ p_1$ and $f_\ominus \circ p_2$. We empirically computed the Fréchet inception distance between the true distribution and the generated distribution using 10000 samples from the true distribution and 5000 samples from the generator distribution.

B.2 GAN'S OBJECTIVE FUNCTION

We used applied DC regularizaiton to the training with the following set of objective functions ($\text{softplus}(x) = \log(1 + \exp(x))$).

GAN-vanilla (Goodfellow et al., 2014)

$$\min_G \max_F \mathbb{E}_\nu[\text{softplus}(F(\boldsymbol{X}))] + \mathbb{E}_{\mu_z}[\text{softplus}(-F(G(\boldsymbol{Z})))] \tag{36}$$

GAN-variant1 (Goodfellow et al., 2014)

$$\max_F \mathbb{E}_\nu[\text{softplus}(F(\boldsymbol{X})] + \mathbb{E}_{\mu_z}[\text{softplus}(-F(G(\boldsymbol{Z})))] \tag{37}$$

$$\min_G \mathbb{E}_{\mu_z}[-\text{softplus}(F(G(\boldsymbol{Z})))] \tag{38}$$

GAN-variant2

$$\max_F \mathbb{E}_\nu[\text{softplus}(F(\boldsymbol{X})] + \mathbb{E}_{\mu_z}[\text{softplus}(-F(G(\boldsymbol{Z})))] \tag{39}$$

$$\min_G \mathbb{E}_{\mu_z}[-F(G(\boldsymbol{Z}))] \tag{40}$$

GAN-hinge (Lim & Ye, 2017)

$$\max_F \mathbb{E}_\nu[\min(0, -1 + F(\boldsymbol{X}))] + \mathbb{E}_{\mu_z}[\min(0, -1 - F(G(\boldsymbol{Z})))] \tag{41}$$

$$\min_G \mathbb{E}_{\mu_z}[-F(G(\boldsymbol{Z}))] \tag{42}$$

WGAN-GP (Gulrajani et al., 2017)

$$\max_F \mathbb{E}_\nu[F(\boldsymbol{X})] - \mathbb{E}_{\mu_z}[F(G(\boldsymbol{Z}))] + \lambda \mathbb{E}_{\hat{\mu}}[(\|\nabla_{\hat{\boldsymbol{X}}} F(\hat{\boldsymbol{X}})\|_2 - 1)^2] \tag{43}$$

$\hat{\mu}$ is the law of $ux + (1-u)z$, with $(x, z, u) \sim \mu \times \nu \times U[0, 1]$.

$$\min_G \mathbb{E}_{\mu_z}[-F(G(\boldsymbol{Z}))] \tag{44}$$

LSGAN (Mao et al., 2017)

$$\min_F \mathbb{E}_\nu[((F(\boldsymbol{X}) - 1)^2] + \mathbb{E}_{\mu_z}[(F(G(\boldsymbol{Z})) + 1)^2] \tag{45}$$

$$\min_G \mathbb{E}_{\mu_z}[(F(G(\boldsymbol{Z})) - 1)^2] \tag{46}$$

Feature Matching (Salimans et al., 2016)

$$\max_F \mathbb{E}_\nu[\min(0, -1 + F(\boldsymbol{X}))] + \mathbb{E}_{\mu_z}[\min(0, -1 - F(G(\boldsymbol{Z})))] \tag{47}$$

$$\min_G ||\mathbb{E}_\nu[\phi(\boldsymbol{X})] - \mathbb{E}_{\mu_z}[\phi(G(\boldsymbol{Z}))]||^2 \tag{48}$$

F is a linear function of ϕ ($\exists w$ with $w^T \phi = F$)

B.3 NETWORK ARCHITECTURES

Table 2: The architecture of DCGAN(Radford et al., 2016) for image Generation experiments on CIFAR-10 and CIFAR-100. The slopes of all leaky-ReLU functions in the networks were set to 0.2.

$\boldsymbol{z} \in \mathbb{R}^{128} \sim \mathcal{N}(0, I)$
dense $\rightarrow M_g \times M_g \times 512$
4×4, stride=2 deconv. BN 256 ReLU
4×4, stride=2 deconv. BN 128 ReLU
4×4, stride=2 deconv. BN 64 ReLU
3×3, stride=1 conv. 3 Tanh

(a) Generator, $M_g = 4$ for CIFAR-10 and CIFAR-100

RGB image $\boldsymbol{x} \in \mathbb{R}^{M \times M \times 3}$
3×3, stride=1 conv 64 lReLU 4×4, stride=2 conv 64 lReLU
3×3, stride=1 conv 128 lReLU 4×4, stride=2 conv 128 lReLU
3×3, stride=1 conv 256 lReLU 4×4, stride=2 conv 256 lReLU
3×3, stride=1 conv. 512 lReLU
dense $\rightarrow$ 1

(b) Discriminator, $M = 32$ for CIFAR10 and CIFAR-100

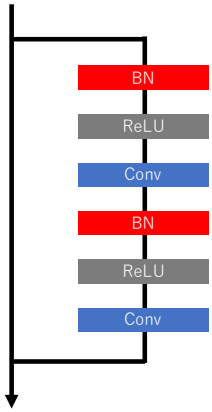

Fig 6: Resblock architectures for CIFAR-10 and CIFAR-100. We used similar architectures as the ones used in Gulrajani et al. (2017)

Table 3: ResNet architectures for CIFAR-10 and CIFAR-100. We used similar architectures as the ones used in Gulrajani et al. (2017).Resblock model is Fig 6

$\boldsymbol{z} \in \mathbb{R}^{128} \sim \mathcal{N}(0, I)$
dense, $4 \times 4 \times 128$
ResBlock up 128
ResBlock up 128
ResBlock up 128
BN, ReLU, 3×3 conv, 3 Tanh

(a) Generator

RGB image $\boldsymbol{x} \in \mathbb{R}^{32 \times 32 \times 3}$
ResBlock down 128
ResBlock down 128
ResBlock 128
ResBlock 128
ReLU
Global sum pooling
dense $\rightarrow$ 1

(b) Discriminator

Table 4: ResNet generator architectures (large version) for CIFAR-10 and CIFAR-100.Resblock model is Fig 6

$\boldsymbol{z} \in \mathbb{R}^{128} \sim \mathcal{N}(0, I)$
dense, $4 \times 4 \times 128$
ResBlock up 256
ResBlock up 256
ResBlock up 256
BN, ReLU, 3×3 conv, 3 Tanh

(a) Generator

Table 5: ResNet architectures for image generation on ImageNet dataset.Resblock model is Fig 6

$\boldsymbol{z} \in \mathbb{R}^{128} \sim \mathcal{N}(0, I)$
dense, $4 \times 4 \times 1024$
ResBlock up 1024
ResBlock up 512
ResBlock up 256
ResBlock up 128
ResBlock up 64
BN, ReLU, 3×3 conv 3
Tanh

(a) Generator

RGB image $\boldsymbol{x} \in \mathbb{R}^{64 \times 64 \times 3}$
ResBlock down 64
ResBlock down 128
ResBlock down 256
ResBlock down 512
ResBlock down 1024
ResBlock 1024
ReLU
Global sum pooling
dense $\rightarrow$ 1

(b) Discriminator for unconditional GANs.

Table 6: EGAN(Dai et al., 2017)'s decoder models used in our experiments on CIFAR-10 and CIFAR-100 . The slopes of all lReLU functions in the networks were set to 0.2. Fig 6 illustrates our Resblock model.

RGB image $\boldsymbol{x} \in \mathbb{R}^{M \times M \times 3}$
3×3, stride=1 conv 64 lReLU 4×4, stride=2 conv 64 lReLU
3×3, stride=1 conv 128 lReLU 4×4, stride=2 conv 128 lReLU
3×3, stride=1 conv 256 lReLU 4×4, stride=2 conv 256 lReLU
3×3, stride=1 conv. 512 lReLU
dense $\rightarrow$ 128 * 2

(a) Convolution decoder, $M = 32$ for CIFAR10 and CIFAR-100

RGB image $\boldsymbol{x} \in \mathbb{R}^{32 \times 32 \times 3}$
ResBlock down 64
ResBlock down 128
ResBlock down 256
ResBlock down 512
ResBlock down 1024
ResBlock 1024
ReLU
Global sum pooling
dense $\rightarrow$ 128 * 2

(b) ResNet decoder.

B.4 DETAILS FOR THE EXPERIMENTS ON CIFAR-10 AND CIFAR-100

Experimental setting for the evaluation of the method's robustness against the choice of objective functions
For the model, we chose the architecture of DCGAN(Radford et al., 2016) (Table 2) and ResNet (Table 3) with spectral normalization applied to full connect layer and convolution layer(SNDCGAN, SNResNet). For the optimization, we used Adam(Kingma & Ba, 2015) and chose $(\alpha = 0.0002, \beta_1 = 0, \beta_2 = 0.9)$ for the hyperparameters. Also, we chose $n_{dis} = 1, n_{gen} = 1$ for SNDCGAN and $(n_{dis} = 5, n_{gen} = 1)$ for SNResNet. We updated the generator $100k$ times and linearly decayed the learning rate over last $5k$ iterations.

Experimental setting for the evaluation of the method's robustness against the choice of the prior dimension
We chose SNDCGAN for the model, and optimized the network with Adam using the hyperparameter $(\alpha = 0.0002, \beta_1 = 0, \beta_2 = 0.9)$. For the update of the discriminator and the generator, we set $n_{dis} = 1, n_{gen} = 1$. We trained the generator $50k$ times and linearly decayed the learning rate over last $5k$ iterations. For the objective function, we chose *GAN-variant2* in Appendix B.2. We also set $\lambda = 3.0, d = 0.01$ for the parameters in (10). For this set of the experiments, we repeated the experiments three times with different seeds, and reported the maximum, mean and minimum. We tested with prior dimensions of range $\dim(\boldsymbol{z}) = 3, 4, 5, 7, 10, 500, 1000, 2000, 4000, 6000, 8000, 10000$.

Comparison with EGAN and other methods
For the model, we chose SNDCGAN , SNResNet and SNResNetLarge, and trained the networks using Adam with hyperparameters $(\alpha = 0.0002, \beta_1 = 0, \beta_2 = 0.9)$. SNResNetLarge is a model that was used in (Miyato et al., 2018). It is a same model as SNResNet except that it is uses a larger generator (Table 4). For both models, We trained the generator $100k$ times and linearly decayed the learning rate over last $10k$ iterations. For EGAN-Ent-VI (Dai et al., 2017), we used an additional decoder equipped with convolution layers. We used $n_{dis} = 1, n_{gen} = 1, n_{dec} = 5$ for SNDCGAN, and $n_{dis} = 1, n_{gen} = 5, n_{dec} = 5$ for SNResNet. The table below is the list of the choices of the hyperparameters (λ, d) in equation (10). we used in our comparative study, sorted by models.

Table 7: List of the hyperparameter choices.

Method	objective	n_{dis}	λ	d
SNDCGAN + DC reg (CIFAR-10)	GAN-variant2	1	3	0
SNDCGAN + DC reg (CIFAR-100)	GAN-variant2	1	3	0
SNDCGAN-hinge + DC reg (CIFAR-10)	GAN-hinge	1	3	0
SNDCGAN-hinge + DC reg (CIFAR-100)	GAN-hinge	1	3	0
SNResNet + DC reg (CIFAR-10)	GAN-variant2	3	3	0
SNResNet + DC reg (CIFAR-100)	GAN-variant2	5	3	0
SNResNetLarge + DC reg (CIFAR-10)	GAN-variant2	5	3	0
SNResNetLarge + DC reg (CIFAR-100)	GAN-variant2	5	4	0
SNResNetLarge-hinge + DC reg (CIFAR-10)	GAN-hinge	5	4	0.01
SNResNetLarge-hinge + DC reg (CIFAR-100)	GAN-hinge	5	4	0.01

B.5 IMAGE GENERATION ON IMAGENET

The images used in this set of experiments were resized to 64×64 pixels. The details of the architecture are given in Table 5. For the optimization, we used Adam with the same hyperparameters we used for ResNet on CIFAR-10 and CIFAR-100 dataset. We trained the networks with 250K generator updates, and applied linear decay for the learning rate after 200K iterations so that the rate would be 0 at the end. We set $\lambda = 6.0, d = 0.01$ for the parameters in equation (10).

C APPENDIX RESULTS

C.1 APPENDIX RESULT ON ARTIFICIAL DATA

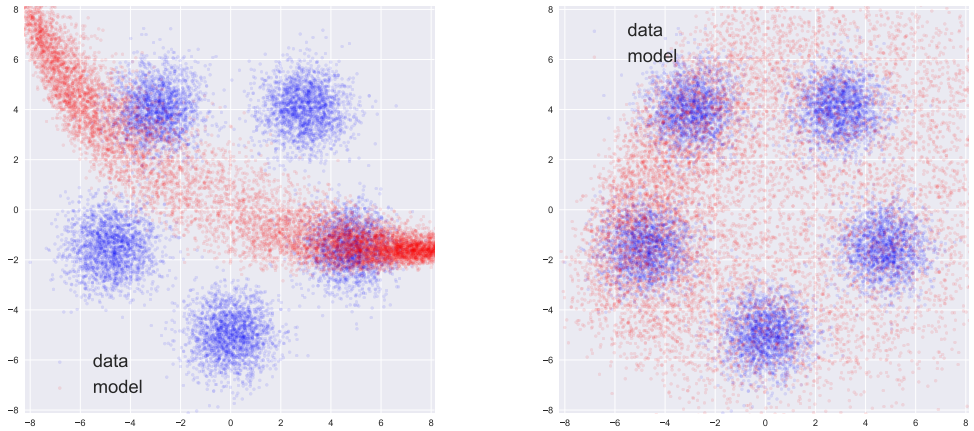

(a) without DC regularization (b) with DC regularization

Fig 7: Generator samples on GMM fitting by GANs (a) without and (b) with DC regularization

C.2 APPENDIX RESULT ON CIFAR-10 AND CIFAR-100

Experiment with different architectures

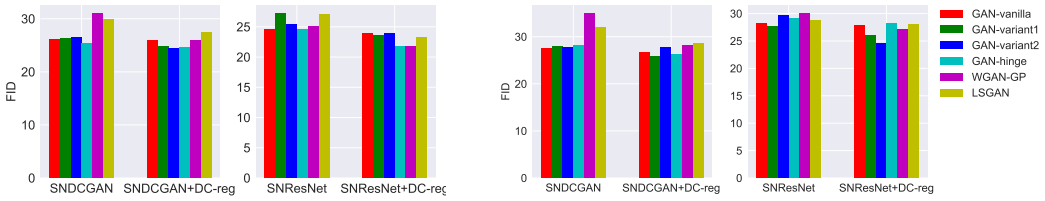

(a) CIFAR-10 (b) CIFAR-100

Fig 8: FIDs for unsupervised image generation on CIFAR-10 and CIFAR-100 (lower the better).

Experiment with different architectures on WGAN-GP

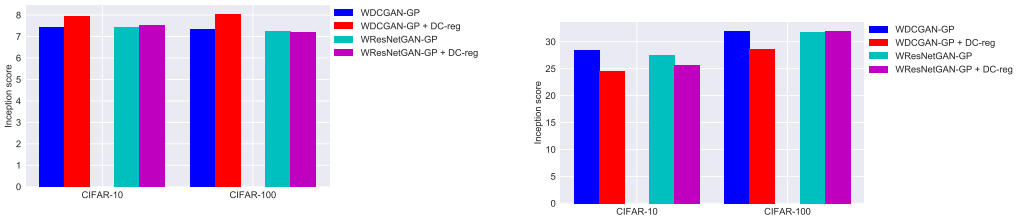

(b) FID(lower is better)

(a) Inception score(higher is better)

Fig 9: Results of WGAN-GP

Experiment with varying prior dimension

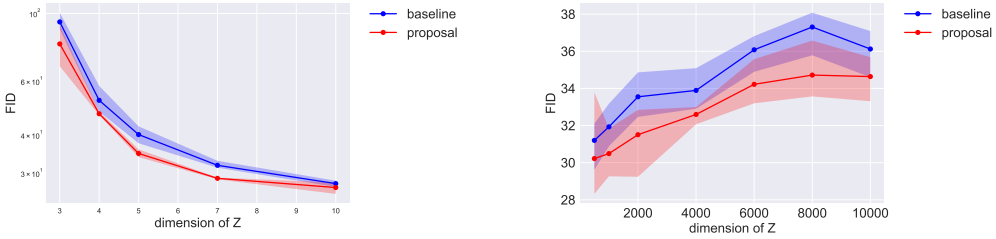

(a) low prior dimension (b) high prior dimension

Fig 10: FID performance of DC regularization on low dimensional prior and high dimensional prior.

Comparison with other methods

Table 8: Inception scores and FIDs with unsupervised image generation on CIFAR-10 and CIFAR-100. CIFAR-10 results for the models designated with † are cited from (Miyato et al., 2018), and the CIFAR-10 results results with ‡ are cited from (Karras et al., 2018). For the details of the objective functions, see Appendix B.2.

Method	**Inception score**		**FID**	
	CIFAR-10	CIFAR-100	CIFAR-10	CIFAR-100
Real data	11.24	14.79	7.6	8.94
EGAN-Ent-VI(SNDCGAN)	6.95±.08	6.62±.10	29.0	33.3
EGAN-Ent-VI(SNResNet)	7.31±.12	6.67±.10	27.0	30.5
feature matching(SNDCGAN)	7.54±.10	7.71±.06	25.9	29.2
proposal				
SNDCGAN + DC reg	8.08±.12	8.12±.11	24.6	25.8
SNDCGAN-hinge + DC reg	7.70±.11	7.99±.09	24.7	26.1
SNResNet + DC reg	8.27±.08	8.27±.13	24.3	24.6
SNResnetLarge + DC reg	8.41±.10	8.20±.08	20.6	24.8
SNResnetLarge-hinge + DC reg	8.29±.09	**8.41**±.11	**19.5**	**23.6**
baseline				
SNDCGAN†	7.42±.08	7.74±.08	29.3	27.9
SNDCGAN-hinge†	7.58±.12	7.57±.07	25.5	28.1
SNResnetLarge-hinge†	8.22±.05	7.54±.13	21.7	26.6
Progressive GANs‡	**8.56**±.06			

Image generation on CIFAR-10 and CIFAR-100

(a) image generation of CIFAR-10

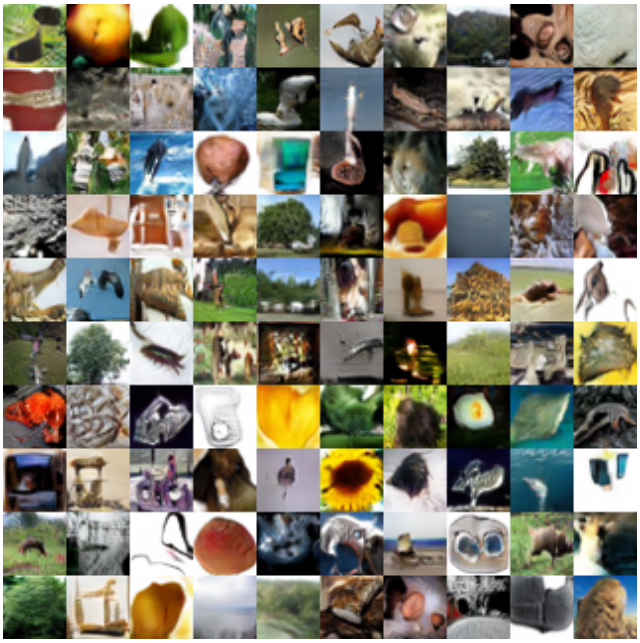

(b) image generation of CIFAR-100

Fig 11: Image generation of CIFAR-10 and CIFAR-100

C.3 APPENDIX RESULT ON IMAGENET

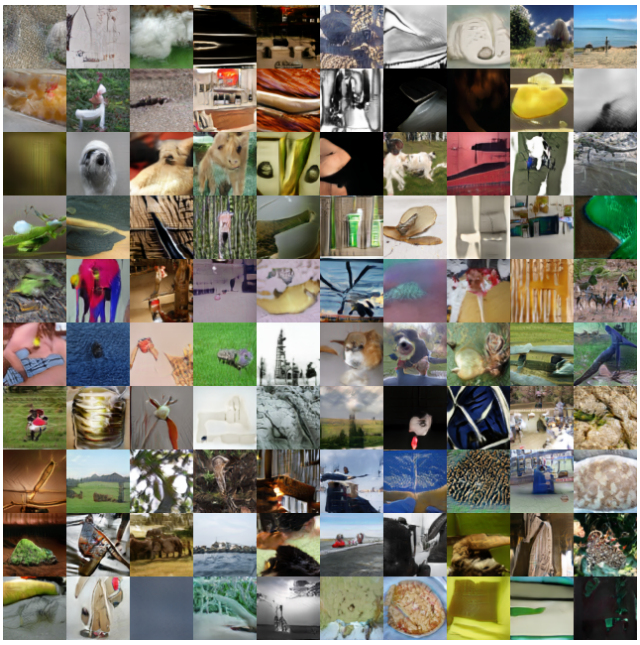

(a) image generation of baseline model

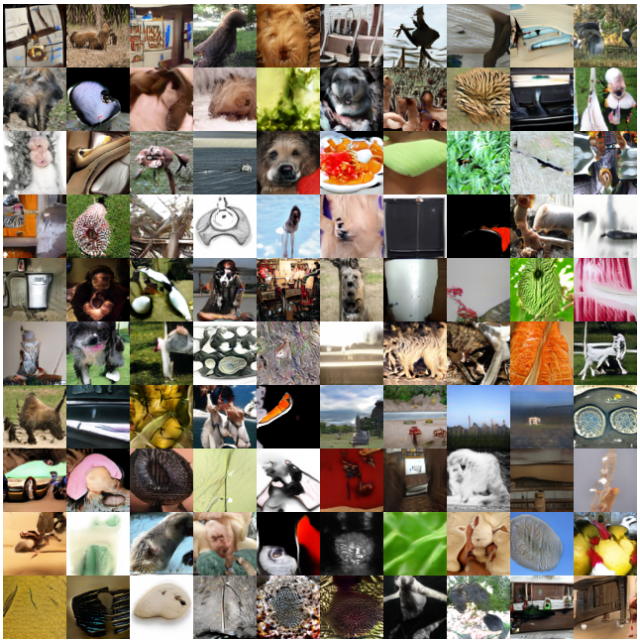

(b) image generation of proposal model

Fig 12: Image generation of ImageNet